

## Proper spatial heterogeneities expand the regime of scale-free behavior in a lattice of excitable elements

Urban Marhl<sup>1,2</sup> and Marko Gosak<sup>1,3,\*</sup>

<sup>1</sup>*Faculty of Natural Sciences and Mathematics, University of Maribor, Koroška cesta 160, SI-2000 Maribor, Slovenia*

<sup>2</sup>*Institute of Mathematics, Physics and Mechanics, Jadranska ulica 19, SI-1000 Ljubljana, Slovenia*

<sup>3</sup>*Institute of Physiology, Faculty of Medicine, University of Maribor, Taborska ulica 8, SI-2000 Maribor, Slovenia*



(Received 25 March 2019; published 12 December 2019)

Signatures of criticality, such as power law scaling of observables, have been empirically found in a plethora of real-life settings, including biological systems. The presence of critical states is believed to have many functional advantages and is associated with optimal operational abilities. Typically, critical dynamics arises in the proximity of phase transition points between absorbing disordered states (subcriticality) and ordered active regimes (supercriticality) and requires a high degree of fine tuning to emerge, which is unlikely to occur in real biological systems. In the present study we propose a rather simple, and biologically relevant mechanism that profoundly expands the critical-like region. In particular, by means of numerical simulation we show that incorporating spatial heterogeneities into the square lattice of map-based excitable oscillators broadens the parameter space in which the distribution of excitation wave sizes follows closely a power law. Most importantly, this behavior is only observed if the spatial profile exhibits intermediate-sized patches with similar excitability levels, whereas for large and small spatial clusters only marginal widening of the critical state is detected. Furthermore, it turned out that the presence of spatial disorder in general amplifies the size of excitation waves, whereby the relatively highest contributions are observed in the proximity of the critical point. We argue that the reported mechanism is of particular importance for excitable systems with local interactions between individual elements.

DOI: [10.1103/PhysRevE.100.062203](https://doi.org/10.1103/PhysRevE.100.062203)

### I. INTRODUCTION

Many real-life systems were found to operate naturally in the vicinity of a critical point, reflecting a transition between order and randomness. This often exerts a spontaneous emergence of self-similar dynamics which embraces a power-law distribution of systems observables [1,2]. While the dynamics of plate tectonics [3,4] and the piling of granular media [5] are probably the most prominent examples of self-organized critical dynamics, similar principles have been identified in a plethora of other real-life complex systems [2,6]. In the last decade, the concepts of phase transition behavior and criticality are increasingly gaining attention also in biological systems research [7,8]. Namely, many living systems are essentially nonlinear and constituted by many interacting elements and as such represent excellent candidates for the emergence of critical dynamics. Even though the exact mechanisms and the underlying principles are incompletely understood [9,10], the number of empirical evidence for scale-invariant behavior in biological settings is increasing, with examples spanning from the microscopic scales of cells and tissues [11–16] to the macroscopic patterns in animal behavior [17,18].

Scale-invariance principles in living matter has received the most attention in the field of neuroscience. Fingerprints of criticality have been identified at different levels of neuronal

organization, ranging from interacting arrays of neurons or astrocytes to the entire brain [16,19–21]. The exact mechanisms for the emergence of critical dynamics in neuronal systems are still under debate and subjected to numerous studies that are based on computational and statistical physics approaches [22–25]. Not only theoretically but also increasingly empirically, critical dynamics are associated with optimized operational abilities of neuronal networks [10,26–29]. Moreover, neuronal population activity might also deviate from the critical regime and exhibit subcritical or supercritical phases, for example during development or pharmacological interventions [30–32]. Notably, recent research suggests that the healthy brain operates near a critical or even slightly subcritical state, thereby ensuring a safety border from supercritical dynamics, which has been associated with pathophysiological behavior, such as epilepsy [33–36].

Typically, critical dynamics emerges at the phase transition between disordered absorbing phase (subcritical behavior) and an active ordered regime (supercritical behavior). In the intermediate regime, long-range spatiotemporal correlated patterns can emerge out of short-range interactions. In networks of excitable elements variations of dynamical states can be induced by changes of global parameters, such as the level of excitability or the interaction strength [22,37–42]. However, an emergent critical behavior is in this case expected only in a very narrow parameter space in the proximity of a phase transition point, which is highly unlikely to occur in real biological systems, since they are

\*marko.gosak@um.si

inherently heterogeneous and operate in a dynamic environment. As plausible mechanisms to overcome this drawback, previous research has underlined the activity-dependent synaptic plasticity, hierarchical network organization, and a balanced interplay between excitatory and inhibitory synapses as the leading neurobiological determinants that drive the neuronal network towards the critical state by means of self-organizing principles [41,43–46]. Noteworthy, intrinsic mechanisms that make such systems hover around critical points have been termed as self-organized quasicriticality and were shown to ensure effective scale invariance across quite a few scales [8].

Realistic neurons and other excitable cells are inherently heterogeneous. They differ in size, morphology, density of receptors, representation of different channels, etc., and exhibit variability in electro-physiological properties and excitability [47]. They are also subjected to rhythmic perturbations [48]. Notably, the intrinsic neuronal diversity was shown to be more than a nuisance and enhances the information processing abilities [49,50]. Often, different types of neurons [51,52], excitable beta cells [53], and channels in myocytes [54] form spatially clustered subpopulations. Motivated by these known physiological characteristics of excitable cells, we analyzed the impact of spatial heterogeneity on the collective activity of excitable cell populations by means of numerical simulations. In particular, we utilized a minimal model of regularly coupled map-based excitable cells and incorporated spatial heterogeneities by means of varying excitability levels. We examined how various levels and configurations of random spatial profiles affected the excitation patterns and critical behavior.

## II. METHODS

### A. Excitable lattice model

We used a phenomenological description of excitable dynamics. In particular, we considered a  $N \times N$  square lattice of coupled Rulkov maps [55]:

$$\begin{aligned} x_{i,j}(t+1) = & \alpha/(1+x_{i,j}(t)^2) + y_{i,j}(t) + D\xi_{i,j} \\ & + \varepsilon[x_{i+1,j}(t) + x_{i-1,j}(t) + x_{i,j-1}(t) \\ & + x_{i,j+1}(t) - 4x_{i,j}(t)], \end{aligned} \quad (1)$$

$$y_{i,j}(t+1) = y_{i,j}(t) - \beta x_{i,j}(t) - \gamma, \quad (2)$$

where  $\alpha$ ,  $\beta$  and  $\gamma$  are the system parameters,  $x_{i,j}(t)$  resembles the membrane potential and  $y_{i,j}(t)$  the ionic recovery currents of the excitable element located in the  $i$ th row and the  $j$ th column of the square lattice,  $t$  is the discrete time index with time step  $\Delta t = 1$ ,  $\xi_{i,j}$  is the Gaussian white noise uncorrelated both in discrete time and space, and  $D$  is the noise intensity. The last term in Eq. (1) stands for the coupling between nearest neighboring elements with  $\varepsilon$  being the coupling strength. The evolution of the variable  $x_{i,j}(t)$  is much faster than  $y_{i,j}(t)$ , due to the small values of the parameters ( $\beta = \gamma = 0.001$ ). When  $\alpha < 2.0$ , one uncoupled unit exhibits a single excitable steady state  $(x^*, y^*) = (-1, -1 - \alpha/2)$ . On the other hand, when  $\alpha > 2.0$ , the steady state loses its stability via a Hopf bifurcation, the model exhibits oscillations and chaotic dynamics

[56]. More detailed analysis was made by the original author of this model [55,57]. In our simulations the initial conditions were  $x_{i,j}(0) = -1.0$  and  $y_{i,j}(0) = -1.995$ , other parameters were set to  $\alpha = 1.95$ ,  $D = 0.005$ ,  $N = 100$ , and we used von Neumann boundary conditions. The coupling strength  $\varepsilon$  was used as a control parameter and was varied between 0 and 0.005.

### B. Spatial heterogeneity

Spatial heterogeneity is a hallmark of many realistic excitable networks. We included this aspect in our model with variations in the excitability level:

$$\alpha_{i,j} = \alpha_0(1 + \Delta\alpha\mu_{i,j}). \quad (3)$$

By this means, each unit in the lattice has a different degree of excitability. In Eq. (3)  $\alpha_0$  is the average excitability ( $\alpha_0 = 1.95$ ),  $\Delta\alpha$  defines the level of heterogeneity and  $\mu_{i,j}$  resembles spatial correlated random number accorded with a two-dimensional Perlin noise [58]. To this purpose,  $m \times m$  random numbers were evenly arranged on our  $N \times N$  square lattice and then continuous functions through all these random values were interpolated. Perlin noise term  $\mu_{i,j}$  is the sum of several interpolated functions with different frequencies ( $b_p^l$ ) and amplitudes ( $1/a_p^l$ ), where  $l$  is an integer representing different harmonics. In our model we calculated the sum of functions for harmonics from  $l = 0$  up to  $l = 4$  and the parameters were  $b_p = 8$  and  $a_p = 8$ . Most importantly, the number of generated random numbers  $m$  determines different forms of spatial heterogeneity [59]. For small values of  $m$  we generated a spatial profile with large clusters of elements with similar excitability levels, whereas higher values yielded smaller spatial subpopulations with similar properties. As  $m \rightarrow N$  the arrangement approaches a spatially uncorrelated random profile. It should be noted that the size of the patches is determined by the  $m/N$  ratio. Irrespective of the Perlin noise parameters, we first normalized the profile  $\mu$  to the unit interval. Next, we subtracted the value of each  $\mu_{i,j}$  with the average value of the whole profile  $\langle \mu \rangle$ . As a result, values of  $\mu_{i,j}$  were within the interval  $[-0.5, 0.5]$ , and the average value of the whole profile was 0, and thus the average excitability level of the whole lattice was always the same:  $\alpha_0 = 1.95$ . Only the intensity of the spatial heterogeneity was varied with the parameter  $\Delta\alpha$ , as explained in Eq. (3). Different types of typical spatial heterogeneities are shown in Fig. 1.

### C. Quantifying the spatiotemporal activity of the excitable lattice

To assess the coherence of spatiotemporal activity profiles we calculated the normalized autocorrelation function of the spatial domain  $x_{i,j}$  at specific times:

$$Y(I, J) = \frac{\langle \tilde{x}_{i,j} \tilde{x}_{i+I, j+J} \rangle}{\sigma^2}, \quad (4)$$

where  $\tilde{x}_{i,j} = x_{i,j} - \langle x_{i,j} \rangle$ ,  $\langle x_{i,j} \rangle$  denotes an average value and  $\sigma^2$  is the variance of the spatial domain  $x_{i,j}$ , calculated as  $\sigma^2 = \langle (x_{i,j}^2) \rangle - \langle x_{i,j} \rangle^2$ .  $I$  and  $J$  represent the spatial lag, i.e., change in the position of a unit in the square lattice from the starting point  $i$  and  $j$ . Autocorrelation indicates the correlation between any two values of the spatial profile with

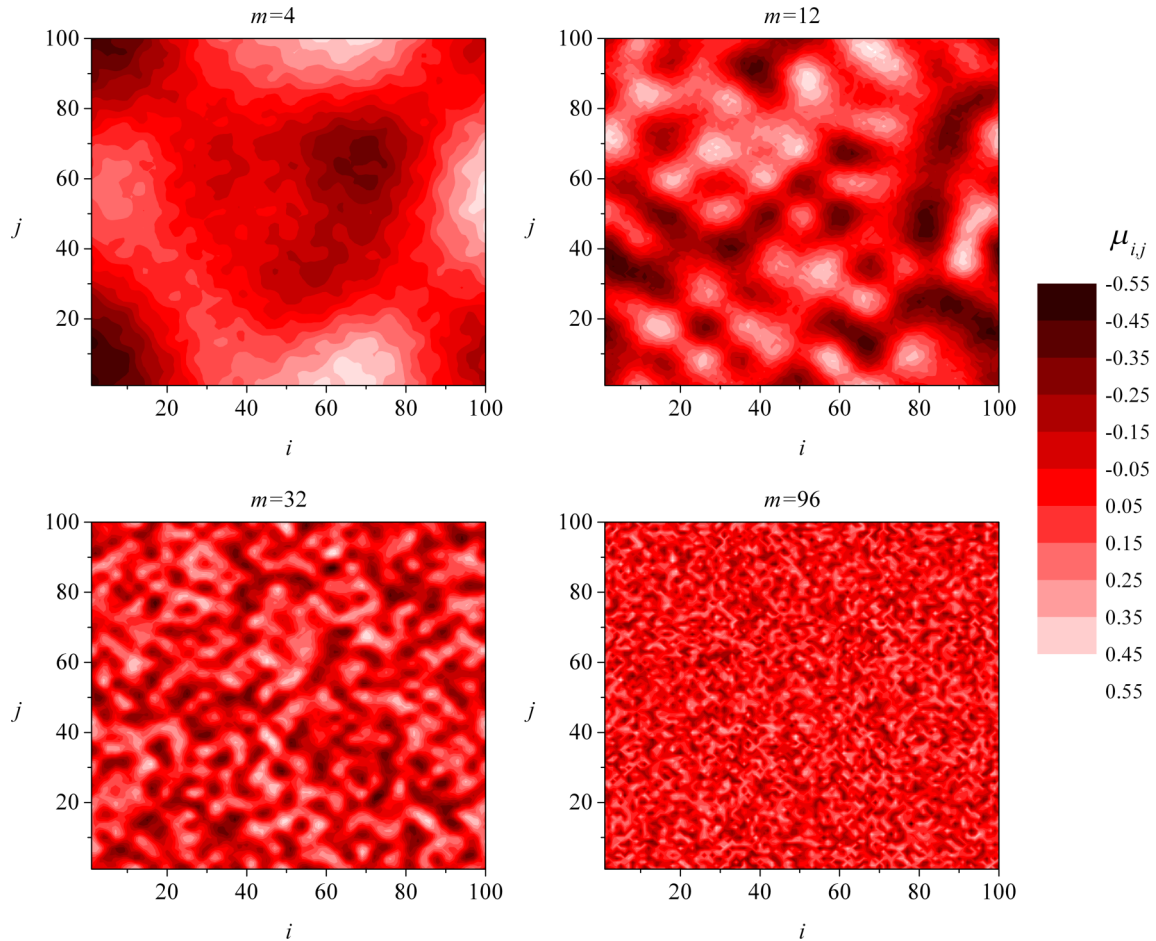


FIG. 1. Perlin noise surfaces as a model of spatial heterogeneities. Color-coded values for the characteristic spatial distribution of  $\mu_{i,j}$  for different values of parameter  $m$ :  $m = 4$ ,  $m = 12$ ,  $m = 32$ , and  $m = 96$ .

respect to the spatial lag. If there are regularities in the spatial domain  $x_{i,j}$ , then the autocorrelation function  $Y(I, J)$  exhibits spatial periodicity and higher values, otherwise, if there is no significant spatial correlation in the analyzed profile,  $Y(I, J)$  monotonically falls to zero, as explained previously [60].

In order to quantify the profiles  $x_{i,j}$  at different time stamps with a single parameter, we calculated the spatial correlation coefficient:

$$R = \frac{1}{(N/4)(N/4)} \sum_{I=1}^{N/4} \sum_{J=1}^{N/4} Y(I, J)^2. \quad (5)$$

High values of  $R$  represents a higher degree of spatial order in the system. The final value of the spatial correlation coefficient for a given parameter set was determined by averaging over 20 000 time stamps and for 15 different runs (spatial profiles).

To identify clusters of active excitable elements and to evaluate the spatiotemporal activity patterns, we first binarized the signals. In particular, an unit of the lattice was considered excited, when the value of the membrane potential at a given time  $[x_{i,j}(t)]$  was greater than the threshold value ( $x_{th} = -0.7$ ). Afterwards, a space-time cluster analysis was performed [13,21,61]. In brief, individual time frames of the binarized lattice were stacked together over an interval

of 20 000 iterations to obtain a space-time cube. Excited elements within this space-time cube formed structures of size  $s$ , which tracked the wave from initiation to cessation. The condition for assigning excited elements to the same cluster was that they were direct neighbors in space or time.

To determine if the dynamics is subcritical, critical or supercritical, we calculated the statistical size distribution. For a given choice of parameters, the distribution was calculated on the basis of 15 independent runs. Irrespective of the choice of parameters, the binning was always selected so that 30 uniform size intervals were attained. The obtained distribution  $P(s)$  was then fitted with the best corresponding power-law function:

$$P(s) = As^k. \quad (6)$$

Both coefficients  $A$  and  $k$  were calculated using the least square method [62]. To determine the goodness of fit ( $\chi^2$ ) we used the Pearson's chi-squared test [63], which summarizes the discrepancy between observed and fitted values. Small values of  $\chi^2$  indicate a good fit, while larger values signify deviation from power-law behavior. In the regime of critical dynamics, the size distribution of the spatiotemporal events follows a power law and hence we used the goodness of fit as an indicator of criticality.

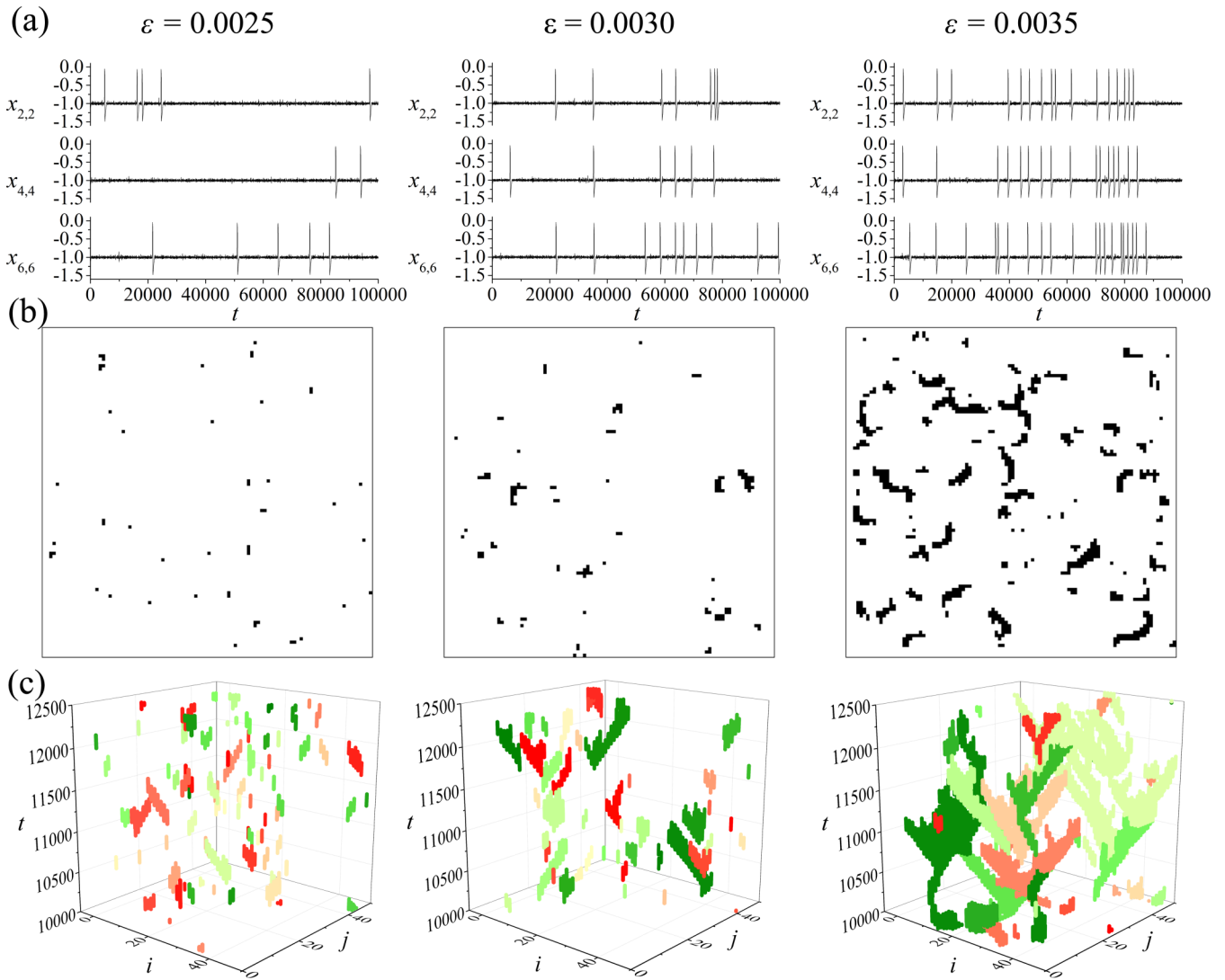


FIG. 2. Spatiotemporal activity of Rulkov maps in square lattice. (a) Time series of membrane potential  $x_{i,j}(t)$  for three different elements of the lattice with indices:  $(i = 2, j = 2)$ ,  $(i = 4, j = 4)$ , and  $(i = 6, j = 6)$ . (b) Snapshots of binarized activity at one specific time, where black dots indicate active units. (c) Space-time plots of the binarized activity patterns. Different colors indicate different excitation waves. All graphics are shown for three values of coupling constant:  $\varepsilon = 0.0025$  (weak coupling),  $\varepsilon = 0.0030$  (intermediate coupling), and  $\varepsilon = 0.0035$  (strong coupling).

### III. RESULTS

We first visualized the spatiotemporal activity of the square lattice network populated with noisy Rulkov maps. In particular, we regarded the coupling strength  $\varepsilon$  as a control parameter and examined how its variations affected the character of excitation waves. Typical temporal traces of the membrane potential activity  $x_{i,j}(t)$  for three selected elements and for three different values of coupling strength are shown in Fig. 2(a). The snapshots of resulting spatial profiles of the excitable lattice are shown in Fig. 2(b), whereas Fig. 2(c) features the corresponding space-time graphs of binarized activity, in which different colors signify individual clusters of activity. Evidently, for weak coupling ( $\varepsilon = 0.0025$ ), only small transitory excitatory patterns emerged that quickly died out. On the other hand, strong coupling ( $\varepsilon = 0.0035$ ) lead to long-lived coherent propagating structures typical for excitable media, which, however, exhibited imperfections and

breakups of waves due to the noisy component. Notably, for the intermediate coupling regime ( $\varepsilon = 0.003$ ), very heterogeneous activity emerged with excitation clusters of very different sizes. These findings corroborate nicely with previous reports [42,61,64].

To gain a deeper insight into the observed behavior, we quantified the spatiotemporal activity patterns by means of spatial autocorrelation. In Fig. 3(a) and Fig. 3(b) we first presented the average spatial autocorrelation functions of the domain  $x$  for the weak and strong coupling strengths, respectively. It can be observed that for the weak coupling regime no spatial correlations were detected, as the spatial autocorrelation monotonically and rather abruptly falls to zero. Apparently, the noise-induced wave nucleations lead in this case only to random spatial structures. On the other hand, for the large coupling, the shape of  $Y(I, J)$  reveals a well-pronounced spatial periodicity, which indicates a high order of coherence and self-similarity in the neuronal dynamics.

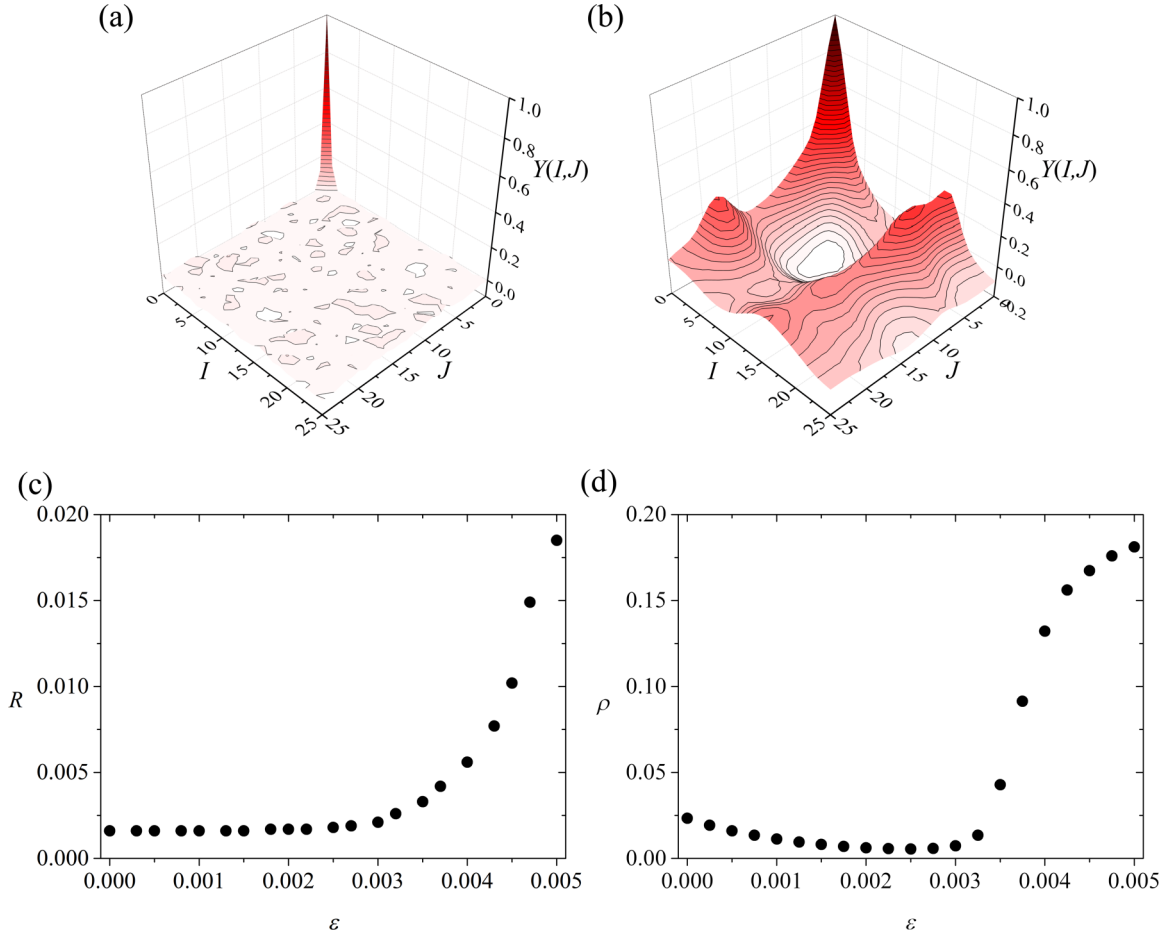


FIG. 3. Autocorrelation of spatial activity patterns in excitable lattices. 2D autocorrelation function  $Y(I, J)$  for selected iteration ( $t$ ) for two values of coupling constant: (a) weak coupling:  $\epsilon = 0.0020$  and (b) strong coupling:  $\epsilon = 0.0045$ . (c) The extent of spatial correlations  $R$  as a function of the coupling constant  $\epsilon$ . (d) The time-averaged network activity  $\rho$  as a function of the coupling constant  $\epsilon$ . Each point in panels (c) and (d) represents the average of 20 000 iterations and 15 independent runs.

To systematically quantify how the spatial coherence varies with coupling strength  $\epsilon$ , we calculated spatial correlation coefficient  $R$  for different values of  $\epsilon$ . The result is shown in Fig. 3(c). As expected, the level of spatial order was found to increase with increasing coupling strength. Most importantly, it appears that a critical value of the coupling parameter exists  $\epsilon \approx 0.0030$ , above which the value of  $R$  rises significantly, thereby signifying the emergence of coherent spatiotemporal activity clusters as this value is exceeded. Moreover, to evaluate this transition with another more elemental measure, we additionally calculated the time averaged network activity:

$$\rho = \left\langle \frac{1}{N^2} \sum X_{Bi}(t) \right\rangle_t, \quad (7)$$

where  $X_{Bi}(t)$  is the binarized activity of the  $i$ th element. The results in Fig. 3(d) indicate that this order parameter behaves very similarly to the spatial correlation coefficient and thereby pinpointing towards the existence of a phase transition point between an absorbing random-like state and an active ordered dynamical regime.

Next, we examined the spatiotemporal dynamics obtained for different values of  $\epsilon$  in the context of criticality and power-law behavior. To this purpose we performed the STC

analysis (see Methods section) and calculated the distribution of excitation cluster sizes  $P(s)$ . The results for three different coupling strengths are shown in Figs. 4(a)–4(c). It can be observed that the distribution of wave sizes is very heterogeneous for all couplings and that the size of waves essentially increases as the coupling is enhanced. Most importantly, the nature of the distribution changes convincingly with variations of the strength of interaction among excitable units. To quantify this visual assessment, we fitted all three distributions with a power-law function. For low and strong coupling, the distribution evidently deviates from a power law. In the first case [Fig. 4(a)], there is a cutoff of larger waves, which indicates subcritical behavior. In the second case [Fig. 4(c)], there is an excess of large excitation clusters, as it is characteristic for supercritical conditions. However, at the intermediate coupling strengths [Fig. 4(b)], the wave size distribution follows very nicely a power-law scaling. A more systematic analysis of the observed behavior was performed by calculating the deviation from an exact power law  $\chi^2$  for different values of  $\epsilon$ . Results in Fig. 4(d) indicate that a scale-free behavior is observed in a narrow parameter space, when the coupling strength is slightly below 0.003. Notably, this critical point roughly corresponds to the phase transition

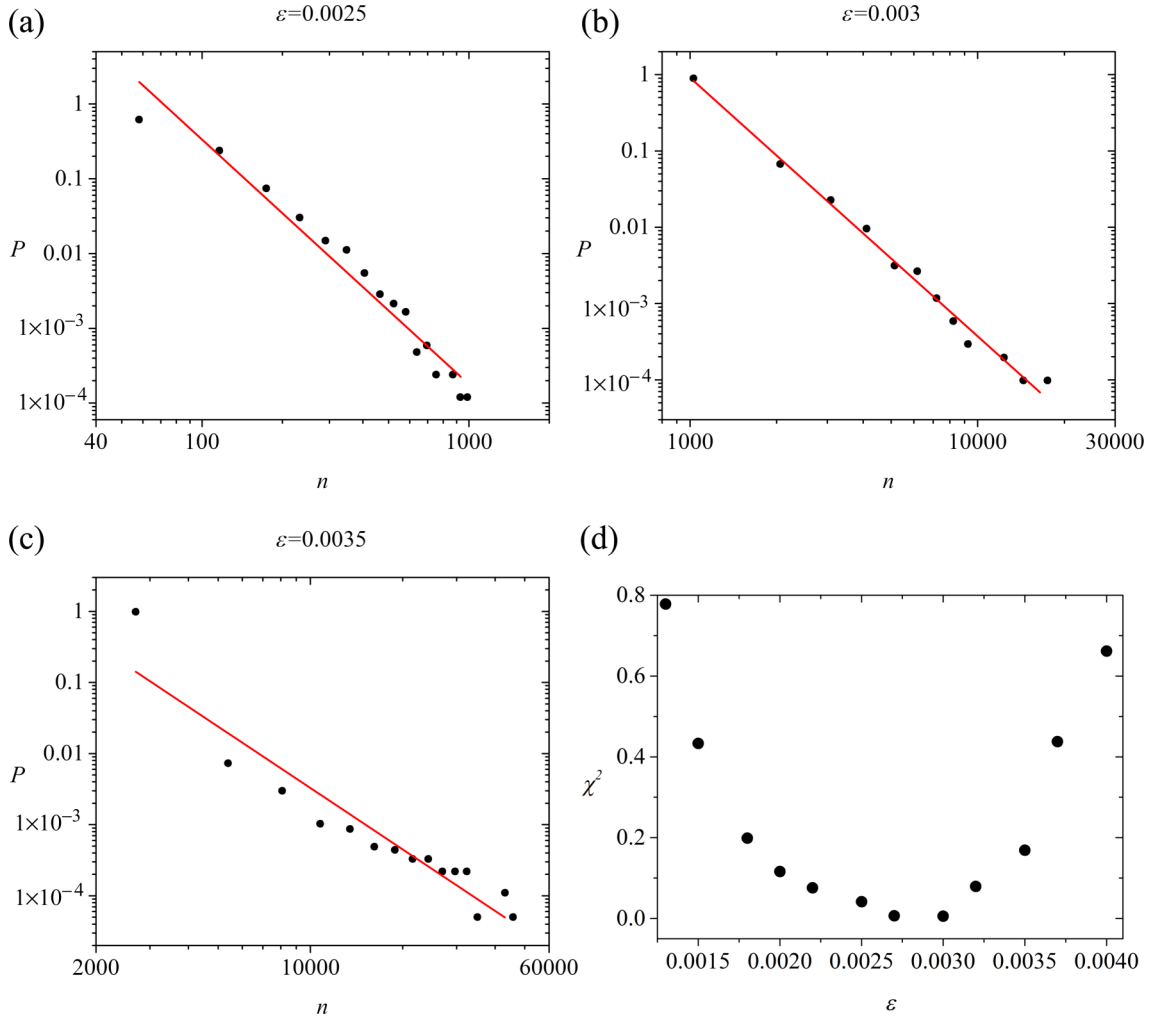


FIG. 4. Distribution of the spatiotemporal excitation wave sizes for weak coupling  $\varepsilon = 0.0025$  (a), intermediate coupling  $\varepsilon = 0.0030$  (b), and strong coupling  $\varepsilon = 0.0035$  (c). The thin red lines show the best power-law fits. The slope of the power-law fit in panel (b) was  $k = -2.8$ . In panel (d) the goodness of fit ( $\chi^2$ ) for fitted power laws as a function of the coupling coefficient are shown, where each point is the average of 15 independent runs.

point observed in Fig. 3(c), in the proximity of which the spatiotemporal dynamics switches from an essentially random to an ordered regime with global waves.

Realistic neurons and other excitable cell types are often inherently heterogeneous, form subpopulations, and differ in among other things in their levels of excitability [13,51]. We therefore examined how spatial heterogeneity impacts the collective dynamics of our computational model of regularly coupled excitable elements with special emphasis on power law behavior. The heterogeneity was implemented by means of variations of the excitability level, as defined in Eq. (3). Most importantly, we investigated the influence of both, the level and the shape of spatial variability. The later was realized by the generation of different 2D Perlin noise profiles on the basis of which values of excitability levels  $\alpha_{i,j}$  were prescribed to individual elements of the lattice. The control parameter  $m$  was used to create qualitatively different spatial profiles (see Fig. 1). Figure 5 shows color-coded values of the deviation from the best matching power-law  $\chi^2$  of the excitation wave sizes distribution as a function of

coupling strength  $\varepsilon$  and heterogeneity level  $\Delta\alpha$ , separately for different spatial profiles. The threshold for scale-free behavior was set to  $\chi^2 < 0.02$  (white color in contour plots). The areas left and right from the critical zone represent the subcritical and supercritical regime, respectively. It can be observed that spatial profiles with smaller patches ( $m \geq 48$ ) the extent of critical regime remains more or less unaffected when the level of heterogeneity rises. Similar, spatial profiles with large patches ( $m \leq 8$ ) also do not broaden the critical regime. In this case only a slight shift towards lower coupling strengths is observed. Remarkably, for intermediate sizes of local regions with similar excitability levels ( $m = 12, 24, 32$ ) a significant expansion of the power-law behavior in parameter space is noticed with increasing extent of spatial disorder.

To provide a more precise insight into the observed behavior, we show in Figs. 6(a)–6(c) cross sections of the contour plots for three different spatial profiles that exhibit large ( $m = 4$ ), intermediate ( $m = 24$ ), and small ( $m = 96$ ) patches of units with similar excitability levels. It can be seen that

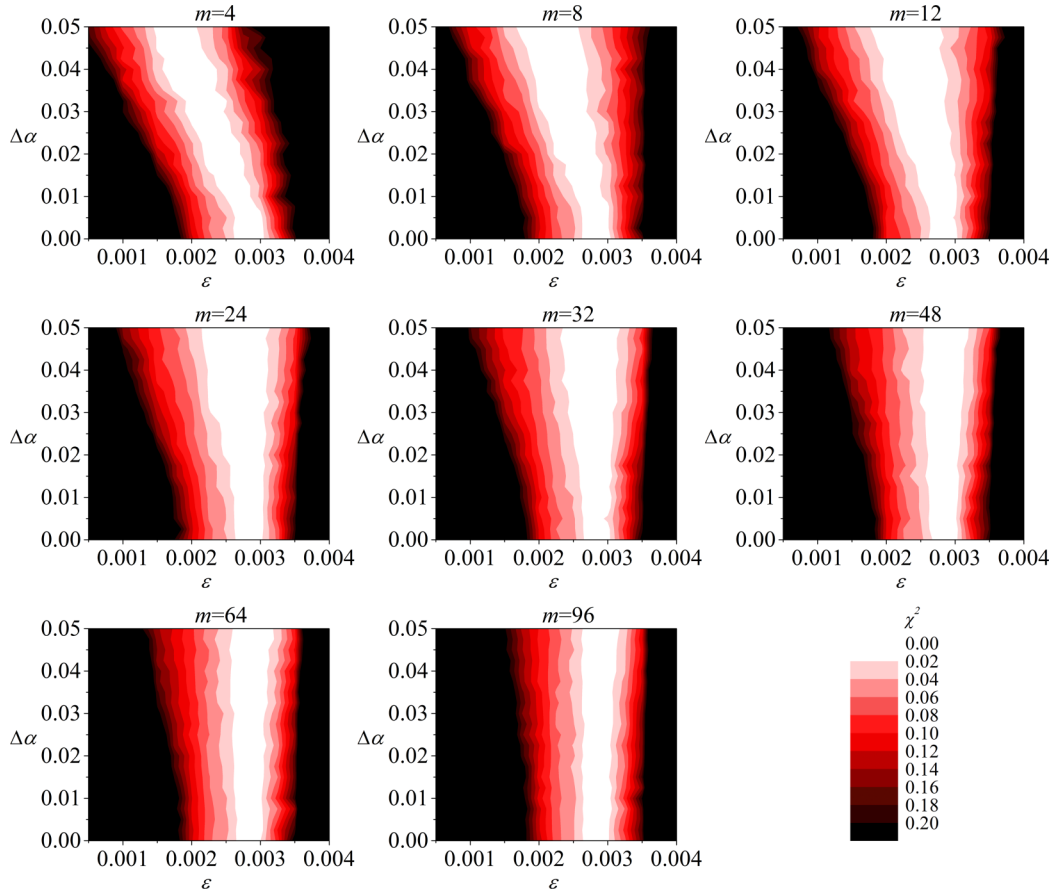


FIG. 5. Regimes of power-law behavior in the heterogeneous excitable lattices. Contour plots show color-coded values of the deviation from the best matching power-law fit of the excitation wave size distributions ( $\chi^2$ ) as a function of the coupling strength ( $\epsilon$ ) and intensity of heterogeneity ( $\Delta\alpha$ ) for different shapes of spatial profiles ( $m$ ).

indeed the broadness of the critical regime indicated by small values of  $\chi^2$  remains unaffected by the heterogeneity for the spatial profile with small [Fig. 6(a)] and large [Fig. 6(c)] patches, whereas for the intermediate profile [Fig. 6(b)] the region with power-law behavior is profoundly expanded and covers a much broader interval of coupling strength values when compared to nonheterogeneous conditions. Finally, we computed the broadness of the critical interval  $\Delta\epsilon_c$  in which the neuronal population operates in the proximity of the scale-free regime ( $\chi^2 \leq 0.02$ ). Figure 6(d) shows how the interval  $\Delta\epsilon_c$  varies with increasing level of heterogeneity  $\Delta\alpha$ . This result confirms that only intermediate sizes of local clusters on the spatial heterogeneity profiles significantly expand the parametric space that leads to power-law scaling of the excitation event sizes.

Finally, to get an intuitive insight into the spatiotemporal behavior of the excitable lattice under the influence of different types of spatial disorder, we plotted in Fig. 7(a) characteristic snapshots of the excitation waves for three different values of  $m$ . It can be observed that for large patches ( $m = 4$ ) the occurrence of waves is solely limited to these high-excitability regions. Since the firing threshold is effectively lower, the behavior switches to criticality already by lower values of the coupling strength (see Fig. 5). However, as the coupling is increased, the wave sizes become large, they often encompass substantial parts of patches, but cannot

propagate between these regions, since the absorbing low-excitability regions are too large as well. The behavior is recognized as supercritical and consequently only a left shift of the critical regime is observed and not a widening. For intermediate-sized patches ( $m = 32$ ), the initiation of waves is still substantially influenced by spatial profiles, but the waves can also travel across the low-excitability regions. As a result, waves with very heterogeneous sizes can therefore be elicited even for higher coupling strengths, which results in a power-law behavior over a wider region of parameter space. In contrast, if the patches are very small ( $m = 96$ ), the nature of excitation waves is weakly affected by the spatial heterogeneities and hence neither a shift or a widening of the scale-free behavior are observed. To further quantify these observations, we plotted in Fig. 7(b) how the average sizes of waves change as a function of the coupling strength. As expected, larger coupling elicits larger waves and larger waves are also provoked by larger patches. In addition, we show in Fig. 7(c) how the spatial disorder affects the relative wave sizes for different values of the coupling strengths. In general, the presence of heterogeneities leads to larger waves when compared to the homogeneous scenario, but, interestingly, the amplification is most pronounced in the proximity of the phase transition point. This observation implies that the excitable lattice is the most prone to spatial perturbations in the proximity of the critical point.

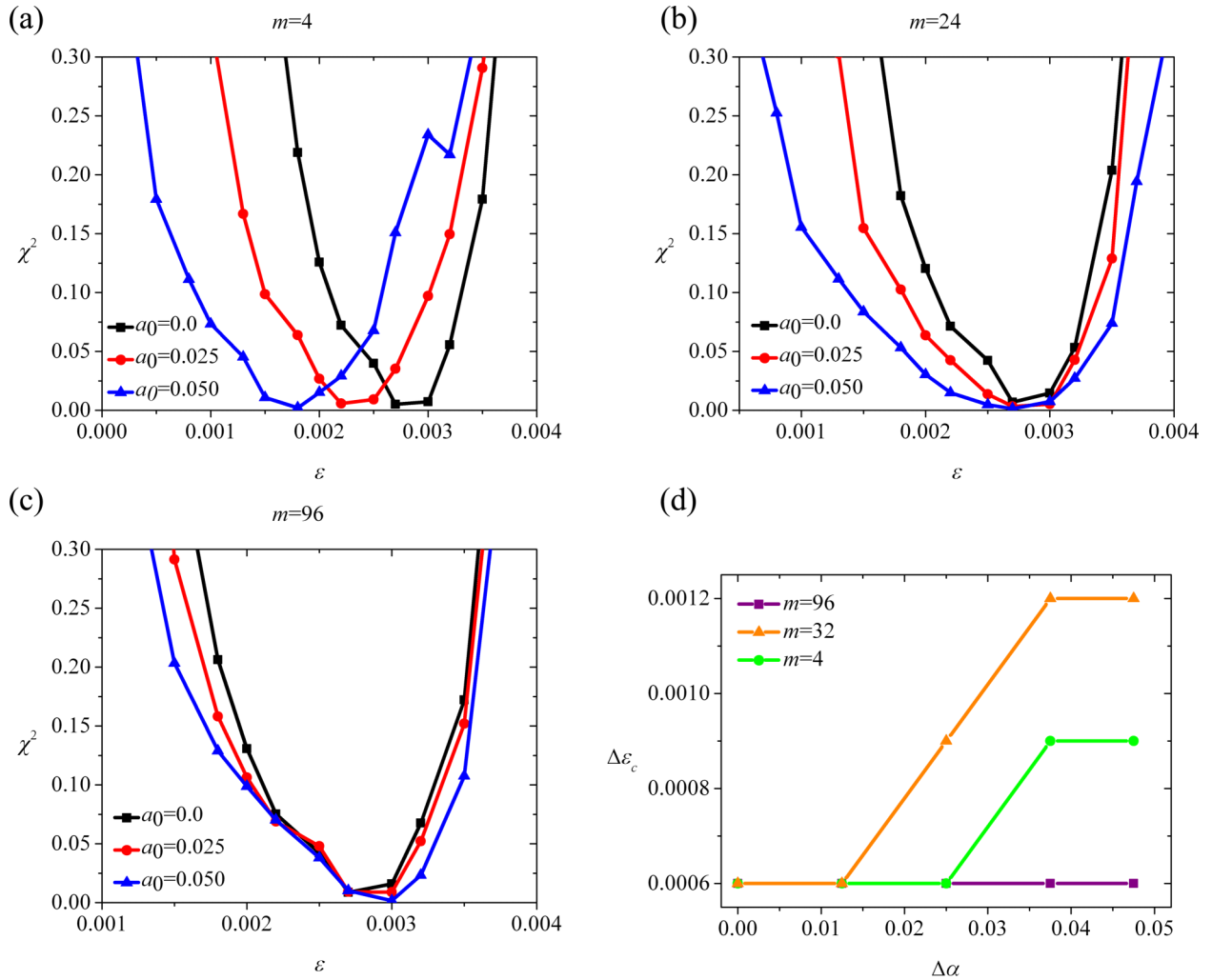


FIG. 6. Assessing the scale-free dynamical regimes in lattices of heterogeneous excitable elements. (a)–(c) The goodness of the best possible power law of the excitation wave sizes  $\chi^2$  as a function of the coupling strength  $\epsilon$  for different characteristics of spatial heterogeneities, defined by parameter  $m$  (see Fig. 1). (d) The width of the parametric space that ensures a scale-free dynamical regime  $\Delta\epsilon_c$  as a function of the level of heterogeneity  $\Delta a$ .

#### IV. DISCUSSION

Information processing in tissues is regulated by large networks of interacting cells. In ensembles of excitable cells, the collective cellular activity is often governed by localized activations, which in turn trigger other elements of the network. Consequently, excitation waves or, in the context of neuroscience also called neuronal avalanches, propagate throughout the system [21]. The resulting dynamics was often found to be scale invariant, as identified by a power-law distribution of the sizes of resulting events. In many recent studies the notion of scale-free behavior of neuronal networks was associated with the presence of critical states [16,20]. Noteworthy, particularly for neuronal systems, many important implications have been found for operating at or near a critical point. In particular, the proximity to critical regimes in neuronal systems is believed to ensure optimal operating abilities and is associated with a normal and healthy function [33,65].

In excitable network models, phase transitions between different dynamical regimes are often associated with a switch from an absorbing (subcritical) state with disorder dynamical

patterns and an active (supercritical) regime characterized with a more regular spatiotemporal activity [22]. It should be noted that in stochastic excitable networks, transitions inferred at the critical parameter values are not critical in a strict sense, but are somehow smeared due to the presence of noise. In general, stochastic perturbations were shown to have a decisive role by shaping the nature of phase transition behavior of coupled excitable oscillators [40,66] as well as on criticality and the distributions of excitation wave sizes [61,67,68]. Furthermore, such nonequilibrium phase transitions between propagating and abortive waves have theoretically been associated with a directed percolation universality class [69–71]. In this vein, variations of some external parameters, such as density of excitable units, coupling strength, noise intensity, or the level of activity, control the spreading of activity, thereby leading the transition from a macroscopically active (percolating) to an inactive (nonpercolating) state [67,72].

In this study, we studied the emergence of self-similar dynamics in a two-dimensional lattice of coupled excitable elements by means of a computational model. We used a map-based description of the excitable dynamics, which is

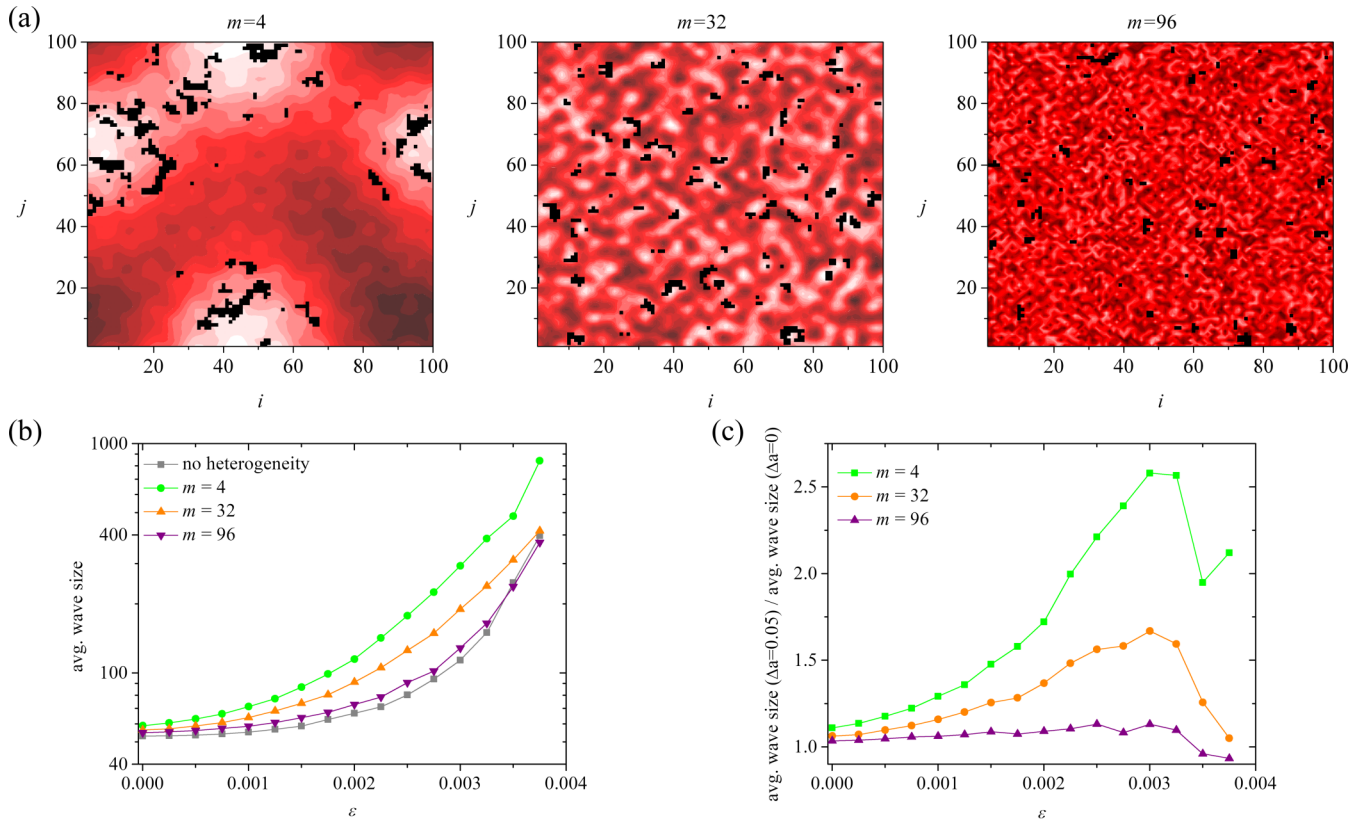


FIG. 7. (a) Color-coded values of Perlin noise profiles for different values of parameter  $m$  with the superimposed snapshot of binarized activity of excitable maps (black dots indicate active units). (b) The average size of excitation waves as a function of the coupling strengths  $\epsilon$  for different types of spatial disorder ( $\Delta a = 0.05$ ) and for the case without spatial heterogeneities. (c) Relative excitation wave sizes as a function of the coupling strength  $\epsilon$  for three different types of spatial profiles. The sizes of waves are normalized with the corresponding values obtained without spatial heterogeneities.

computationally more efficient than its time-continuous counterparts, and thus presents a more appropriate environment for simulations on larger spatial and temporal scales [73]. We were particularly interested in the presence and robustness of scale-invariant dynamics. As expected, we detected critical behavior in a very narrow parameter space in the proximity of a phase transition towards an ordered and active dynamical state. However, since realistic excitable cells are in general heterogeneous and they function in changing environments, fine-tuning of parameters is not expected to be an efficient mechanism for ensuring criticality in real-life settings. In the neuroscientific community, one of the main issues about criticality are therefore the mechanisms that ensure a robust critical state of the network. Many studies put forward the idea that dynamical and activity-dependent synapses are one of the leading neurobiological factors that ensure critical dynamics [41,74,75]. Moreover, several authors have shown that a complex interaction structure can act as an effective promoter of scale-free behavior [31,76], especially when the hierarchical-modular architecture of cortical networks is taken into account [44,45,77,78]. However, it should be noted most of these neuronal network models are composed by nonconservative elements and are therefore not critical in a strict sense. They often encompass some self-organizing principles that make them hover around the critical point. This kind of behavior is termed as self-organized quasicriticality and is

able to create effective scale invariance across quite a few scales [79,80]. In contrast, our model does not contain any self-organisation or adaptation. Scale-invariant behavior can only be inferred by the precise selection of parameters, yet the inclusion of spatial disorder was found to profoundly enlarge the pseudocritical region. Previously, the questions how to expand the power-law behavior over broader scales has already been addressed by Kinouchi and Prado [81]. Furthermore, another route to broad regions of critical-like features are the so-called Griffiths phases [82]. Moretti and Muñoz [44] have shown that quenched disorder smears the parameter space which leads to the emergence of a generic scale invariance in hierarchically modular networks. Later, these ideas have been generalized to nonhierarchical modular networks as well [83] and verified numerically in a large scale connectome model [84]. It has been argued that for biological systems it might suffice to operate in such phases without the need to invoke precise tuning to the edge of a phase transition to obtain functional benefits stemming from spatiotemporal scale invariance [8].

In contrast to previous endeavors that were focused mainly on nontrivially structured and heterogeneous excitable networks, we investigated the possibilities for broadening the region of scale-invariant behavior of excitation waves in a regular square lattice of excitable elements. Namely, in many realistic cells and tissues, the interactions among excitable

elements are mostly limited to nearest neighbors only, such as in cardiac myocytes [14], oocytes [85], or between pancreatic beta cells [13], and were shown to exhibit fingerprints of self-organized criticality as well. Even neuronal tissue might exhibit a regular lattice-like axonal connectivity at the scale of small neuronal populations or in the early evolutionary stages [86,87]. Within the excitable cell membranes, such as on cardiac smooth muscle cells or oocytes, criticality has been argued as a gateway to whole-cell oscillations, whereby in the critical regime local single-channel fluctuations and  $\text{Ca}^{2+}$  sparks can successfully evolve to whole-cell oscillations. On the other hand, in the subcritical regime, i.e., below the phase transition point, local random excitations do not evolve to large scale wave formation [14,85,88]. It should be noted that such a transition from local to global signals has theoretically been associated with a directed percolation universality class, as explained above [70–72]. Moreover, in pancreatic islets of Langerhans, the main synchronizing mechanisms is the electrical coupling through rather regular gap junctional networks which ensure calcium wave propagation across the tissue. However, cellular heterogeneity, the existence of subpopulations and other communication mechanisms within islets introduce certain spatial disorder that contributes to complex collective activity patterns, which in certain regimes exhibit fingerprints of criticality [13,42].

Noteworthy, our computational results have revealed that the incorporation of spatial heterogeneities, a genuine characteristic of many excitable settings, affects profoundly the spatiotemporal activity. In particular, proper spatial hetero-

geneity profiles that are characterized with intermediate-sized clusters with similar excitability levels, profoundly expand the parameter space region in which the distribution of excitation wave sizes follows closely a power law. We argue that the presence of properly scaled patches introduces a modular spatial structure, in which the nucleation of waves occurs more often in patches with elevated excitability. If the sizes of these patches are properly scaled, this affects the excitation wave decay profiles in the way that they can exhibit heterogeneous self-similar behavior over broad intervals.

To conclude, the occurrence of spatial heterogeneities in realistic excitable systems can for example be linked with regional subcellular heterogeneities in ATP-sensitive potassium channels [89], spatially clustered neuronal subpopulations with similar features [51,52], or spatial organization of pancreatic beta cell subpopulations [53]. If the intrinsic structural heterogeneities of various excitable systems are properly scaled and organized, they can be considered as an important factor for ensuring a more robust critical-like behavior. Our findings thus discerned an intriguing association between structural organization and dynamics of excitable systems in which the emergent wave activity is mediated by local interactions.

#### ACKNOWLEDGMENT

The authors acknowledge the financial support from the Slovenian Research Agency (research core funding, P3-0396 and P2-0348).

- 
- [1] P. Bak, C. Tang, and K. Wiesenfeld, *Phys. Rev. A* **38**, 364 (1988).
  - [2] D. Marković and C. Gros, *Phys. Rep.* **536**, 41 (2014).
  - [3] P. Bak, *How Nature Works: The Science of Self-Organized Criticality* (Copernicus, New York, 1999).
  - [4] B. Gutenberg and C. F. Richter, *Ann. Geophys.* **9**, 1 (1956).
  - [5] V. Frette, K. Christensen, A. Malthe-Sørensen, J. Feder, T. Jøssang, and P. Meakin, *Nature (London)* **379**, 49 (1996).
  - [6] K. Yara, F. Eliseo, S. Pieter, and H. Cristián, *J. R. Soc. Interface* **14**, 20170662 (2017).
  - [7] T. Mora and W. Bialek, *J. Stat. Phys.* **144**, 268 (2011).
  - [8] M. A. Muñoz, *Rev. Mod. Phys.* **90**, 031001 (2018).
  - [9] R. Frigg, *Stud. Hist. Philos. Sci. Part A* **34**, 613 (2003).
  - [10] E. Lovecchio, P. Allegrini, E. Geneston, B. J. West, and P. Grigolini, *Front. Physiol.* **3**, 98 (2012).
  - [11] P. Allegrini, P. Paradisi, D. Menicucci, M. Laurino, A. Piarulli, and A. Gemignani, *Phys. Rev. E* **92**, 032808 (2015).
  - [12] M. A. Aon, S. Cortassa, and B. O'Rourke, *Proc. Natl. Acad. Sci. USA* **101**, 4447 (2004).
  - [13] M. Gosak, A. Stožer, R. Marković, J. Dolenšek, M. Perc, M. S. Rupnik, and M. Marhl, *Front. Physiol.* **8**, 1106 (2017).
  - [14] M. Nivala, C. Y. Ko, M. Nivala, J. N. Weiss, and Z. Qu, *Biophys. J.* **102**, 2433 (2012).
  - [15] M. Nykter, N. D. Price, M. Aldana, S. A. Ramsey, S. A. Kauffman, L. E. Hood, O. Yli-Harja, and I. Shmulevich, *Proc. Natl. Acad. Sci. USA* **105**, 1897 (2008).
  - [16] D. Plenz and T. C. Thiagarajan, *Trends Neurosci.* **30**, 101 (2007).
  - [17] W. Bialek, A. Cavagna, I. Giardina, T. Mora, E. Silvestri, M. Viale, and A. M. Walczak, *Proc. Natl. Acad. Sci. USA* **109**, 4786 (2012).
  - [18] B. C. Daniels, D. C. Krakauer, and J. C. Flack, *Nat. Commun.* **8**, 14301 (2017).
  - [19] J. M. Beggs and D. Plenz, *J. Neurosci.* **23**, 11167 (2003); **23**, 2433 (2012).
  - [20] J. Hesse and T. Gross, *Front. Syst. Neurosci.* **8**, 166 (2014).
  - [21] P. Jung, A. Cornell-Bell, K. S. Madden, and F. Moss, *J. Neurophysiol.* **79**, 1098 (1998).
  - [22] L. Brochini, A. de Andrade Costa, M. Abadi, A. C. Roque, J. Stolfi, and O. Kinouchi, *Sci. Rep.* **6**, 35831 (2016).
  - [23] M. Martinello, J. Hidalgo, A. Maritan, S. di Santo, D. Plenz, and M. A. Muñoz, *Phys. Rev. X* **7**, 041071 (2017).
  - [24] G. Tkačik, T. Mora, O. Marre, D. Amodei, S. E. Palmer, M. J. Berry, and W. Bialek, *Proc. Natl. Acad. Sci. USA* **112**, 11508 (2015).
  - [25] M. Zare and P. Grigolini, *Chaos Solitons Fractals* **55**, 80 (2013).
  - [26] C. Haldeman and J. M. Beggs, *Phys. Rev. Lett.* **94**, 058101 (2005).
  - [27] O. Kinouchi and M. Copelli, *Nat. Phys.* **2**, 348 (2006).
  - [28] W. L. Shew, H. Yang, S. Yu, R. Roy, and D. Plenz, *J. Neurosci. Off. J. Soc. Neurosci.* **31**, 55 (2011).
  - [29] R. Stoop and F. Gomez, *Phys. Rev. Lett.* **117**, 038102 (2016).
  - [30] J. Barral and A. D Reyes, *Nat. Neurosci.* **19**, 1690 (2016).

- [31] P. Massobrio, V. Pasquale, and S. Martinoia, *Sci. Rep.* **5**, 10578 (2015).
- [32] C. Tetzlaff, S. Okujeni, U. Egert, F. Wörgötter, and M. Butz, *PLoS Comput. Biol.* **6**, e1001013 (2010).
- [33] P. Massobrio, L. de Arcangelis, V. Pasquale, H. J. Jensen, and D. Plenz, *Front. Syst. Neurosci.* **9**, 22 (2015).
- [34] C. Meisel, A. Storch, S. Hallmeyer-Elgner, E. Bullmore, and T. Gross, *PLoS Comput. Biol.* **8**, e1002312 (2012).
- [35] V. Priesemann, *Front. Syst. Neurosci.* **8**, 108 (2014).
- [36] N. Tomen, D. Rotermund, and U. Ernst, *Front. Syst. Neurosci.* **8**, 151 (2014).
- [37] S. Bornholdt and T. Röhl, *Phys. Rev. E* **67**, 066118 (2003).
- [38] M. Dehghani-Habibabadi, M. Zare, F. Shahbazi, J. Usefie-Mafahim, and P. Grigolini, *Eur. Phys. J. E* **40**, 101 (2017).
- [39] Y. Kuramoto, *Phys. Nonlinear Phenom.* **50**, 15 (1991).
- [40] K.-E. Lee, M. A. Lopes, J. F. F. Mendes, and A. V. Goltsev, *Phys. Rev. E* **89**, 012701 (2014).
- [41] A. Levina, J. M. Herrmann, and T. Geisel, *Nat. Phys.* **3**, 857 (2007).
- [42] A. Stožer, R. Markovič, J. Dolenšek, M. Perc, M. Marhl, M. Slak Rupnik, and M. Gosak, *Front. Physiol.* **10**, 869 (2019).
- [43] João Guilherme Ferreira Campos, A. de A. Costa, M. Copelli, and O. Kinouchi, *Phys. Rev. E* **95**, 042303 (2017).
- [44] P. Moretti and M. A. Muñoz, *Nat. Commun.* **4**, 2521 (2013).
- [45] M. Rubinov, O. Sporns, J.-P. Thivierge, and M. Breakspear, *PLoS Comput. Biol.* **7**, e1002038 (2011).
- [46] S.-J. Wang, C. C. Hilgetag, and C. Zhou, *Front. Comput. Neurosci.* **5**, 30 (2011).
- [47] Q. Liu, E. Lee, and R. L. Davis, *Neuroscience* **257**, 96 (2014).
- [48] S. A. Moosavi, A. Montakhab, and A. Valizadeh, *Phys. Rev. E* **98**, 022304 (2018).
- [49] M. I. Chelaru and V. Dragoi, *Proc. Natl. Acad. Sci. USA* **105**, 16344 (2008).
- [50] K. Padmanabhan and N. N. Urban, *Nat. Neurosci.* **13**, 1276 (2010).
- [51] D. A. Dombeck, M. S. Graziano, and D. W. Tank, *J. Neurosci.* **29**, 13751 (2009).
- [52] R. Dubourget, A. Sangare, H. Geoffroy, T. Gallopin, and A. Rancillac, *Brain Struct. Funct.* **222**, 1153 (2017).
- [53] M. J. Westacott, N. W. F. Ludin, and R. K. P. Benninger, *Biophys. J.* **113**, 1093 (2017).
- [54] A. Bhargava, X. Lin, P. Novak, K. Mehta, Y. Korchev, M. Delmar, and J. Gorelik, *Circ. Res.* **112**, 1112 (2013).
- [55] N. F. Rulkov, *Phys. Rev. E* **65**, 041922 (2002).
- [56] M. Perc, *Chaos Solitons Fractals* **31**, 64 (2007).
- [57] N. F. Rulkov, *Phys. Rev. Lett.* **86**, 183 (2001).
- [58] K. Perlin, in *Proceedings of the 12th Annual Conference on Computer Graphics and Interactive Techniques* (ACM, New York, 1985), pp. 287–296.
- [59] M. Fras and M. Gosak, *Biosystems* **114**, 172 (2013).
- [60] M. Gosak, *Biophys. Chem.* **139**, 53 (2009).
- [61] P. Jung, *Phys. Rev. Lett.* **78**, 1723 (1997).
- [62] W. H. Press, S. A. Teukolsky, W. T. Vetterling, and B. P. Flannery, *Numerical Recipes 3rd Edition: The Art of Scientific Computing*, 3rd ed. (Cambridge University Press, Cambridge, 2007).
- [63] K. Pearson, in *Breakthroughs in Statistics: Methodology and Distribution*, edited by S. Kotz and N. L. Johnson (Springer, New York, 1992), pp. 11–28.
- [64] F. Sagués, J. M. Sancho, and J. García-Ojalvo, *Rev. Mod. Phys.* **79**, 829 (2007).
- [65] W. L. Shew, W. P. Clawson, J. Pobst, Y. Karimipannah, N. C. Wright, and R. Wessel, *Nat. Phys.* **11**, 659 (2015).
- [66] B. Lindner, *Phys. Rep.* **392**, 321 (2004).
- [67] M. H. Hennig, C. Adams, D. Willshaw, and E. Sernagor, *J. Neurosci.* **29**, 1077 (2009).
- [68] A. Neiman, L. Schimansky-Geier, A. Cornell-Bell, and F. Moss, *Phys. Rev. Lett.* **83**, 4896 (1999).
- [69] H. Hinrichsen, *Adv. Phys.* **49**, 815 (2000).
- [70] S. Coombes and Y. Timofeeva, *Phys. Rev. E* **68**, 021915 (2003).
- [71] N. Guisoni and M. J. de Oliveira, *Phys. Rev. E* **74**, 061905 (2006).
- [72] Y. Timofeeva and S. Coombes, *Phys. Rev. E* **70**, 062901 (2004).
- [73] M. Girardi-Schappo, M. H. R. Tragtenberg, and O. Kinouchi, *J. Neurosci. Methods* **220**, 116 (2013).
- [74] A. de A. Costa, M. Copelli, and O. Kinouchi, *J. Stat. Mech.* (2015) P06004.
- [75] L. Michiels van Kessenich, L. de Arcangelis, and H. J. Herrmann, *Sci. Rep.* **6**, 32071 (2016).
- [76] M. Lin and T. L. Chen, *Phys. Rev. E* **71**, 016133 (2005).
- [77] S. Valverde, S. Ohse, M. Turalaska, B. J. West, and J. Garcia-Ojalvo, *Front. Physiol.* **6**, 127 (2015).
- [78] S.-J. Wang and C. Zhou, *New J. Phys.* **14**, 023005 (2012).
- [79] J. A. Bonachela, S. de Franciscis, J. J. Torres, and M. A. Muñoz, *J. Stat. Mech.* (2010) P02015.
- [80] O. Kinouchi, L. Brochini, A. A. Costa, J. G. F. Campos, and M. Copelli, *Sci. Rep.* **9**, 3874 (2019).
- [81] O. Kinouchi and C. P. C. Prado, *Phys. Rev. E* **59**, 4964 (1999).
- [82] A. G. Moreira and R. Dickman, *Phys. Rev. E* **54**, R3090 (1996).
- [83] W. Cota, G. Ódor, and S. C. Ferreira, *Sci. Rep.* **8**, 9144 (2018).
- [84] G. Ódor, *Phys. Rev. E* **99**, 012113 (2019).
- [85] L. Lopez, E. Piegari, L. Sigaut, and S. Ponce Dawson, *Front. Physiol.* **3**, 350 (2012).
- [86] M. Kaiser and S. Varier, *Netw. Comput. Neural Syst.* **22**, 143 (2011).
- [87] M.-T. Hütt, M. Kaiser, and C. C. Hilgetag, *Philos. Trans. R. Soc. B Biol. Sci.* **369**, 20130522 (2014).
- [88] R. Thul, S. Coombes, H. L. Roderick, and M. D. Bootman, *Proc. Natl. Acad. Sci. USA* **109**, 2150 (2012).
- [89] M. Hong, L. Bao, E. Kefaloyianni, E. Agullo-Pascual, H. Chkourko, M. Foster, E. Taskin, M. Zhandre, D. A. Reid, E. Rothenberg, M. Delmar, and W. A. Coetzee, *J. Biol. Chem.* **287**, 41258 (2012).